Arabian Journal of Chemical and Environmental Research

Vol. 13 Issue 2 (2026) 326–351

Sequential Extraction of Potentially Toxic Elements and their Health Risks in Soils around Rimin Gado Granite Quarry Sites, Kano State, Nigeria

A. M. Mahmud[1]* M. S. Musa[2,3] Z. Abdullahi[3], A. Twaha[2], and S.Y. Sule[1]

[1]*Department of Chemistry, Faculty of Science. Aliko Dangote University of Science and Technology, Wudil, Nigeria. PMB 3244. Emai: linfo@kustwudil.edu.ng*

[2]*Department of Chemistry and Biochemistry, Faculty of Science, Islamic University in Uganda, Mbale, Uganda PMB 2555 Email: info@iuiu.ac.ug*

[3]*Department of Pure and Industrial Chemistry, Faculty of Science, Bayero University, Kano, Nigeria. PMB 3011 Email: bukinfo@buk.edu.ng*

Email : ashir@kustwudil.edu.ng, msmusa.chm@buk.edu.ng

Received 01 November 2026, Revised 26 xxx 2026, Accepted 26 xxx 2026

Cited as: *Mahmud A.M., Musa M.S., Abdullahi Z., Twaha A., Sule S.Y. (2026). Sequential Extraction of Potentially Toxic Elements and their Health Risks in Soils around Rimin Gado Granite Quarry Sites, Kano State, Nigeria, Arab. J. Chem. Environ. Res. 13(2), 326-351*

Abstract

This study investigated the distribution, speciation, and health risks of potentially toxic elements (PTEs) in soils surrounding the Rimin Gado granite quarry, Kano State, Nigeria, using sequential extraction and pollution assessment indices. Soil samples collected from nine sites revealed pronounced spatial variability, with pseudo-total metal concentrations decreasing in the order QS > ZS > DG > HM > ZD > SC > BK > KT > CR. The total fractions was obtained by adding all metals concentrations in water soluble, exchangeable, reducible, oxidizable and residual fraction respectively. Mean concentrations (mg/kg) at the quarry site (QS) were notably elevated for Fe (215.12), Al (228.67), Zn (225.12), Pb (30.56), Cr (87.04), Ni (141.19), As (33.39),Co (98.7), Mn (197.83), Cu (134.78) and Cd (3.95), compared to control values Fe (82.25), Zn (64.26), Al (174.0), Pb (5.25), Cr (36.97), Ni (87.34), As (7.4),Co (57.36), Mn (150.2), Cu (90.02) and Cd (0.015). Sequential extraction showed that Cd (65%), Pb (52%), and Zn (48%) were predominantly associated with labile fractions (water-soluble, exchangeable, and carbonate-bound), indicating high mobility and bioavailability, whereas Fe and Al (>85%) resided in the residual fraction, confirming lithogenic origin. Pollution indices revealed considerable to very high contamination for Cd (CF: 6.2–9.8) and moderate contamination for Pb and As. Geo-accumulation index (Igeo) classified Cd as moderately to heavily polluted at quarry-proximal sites. Health risk assessment indicated that hazard index (HI) values exceeded unity for children at QS (HI = 2.31) and BK (HI = 1.76), driven primarily by As, Cd and Pb exposure. Carcinogenic risk (TCR) values for As, and Cd ranged from 1.2×10^{-4} to 3.8×10^{-4} at impacted sites, exceeding acceptable thresholds.

Keywords: Granite, Quarry, Sequential extraction, Pollution indexes, Carcinogenic, Health risk

*Corresponding author. *E-mail address: ashir@kustwudil.edu.ng*

1. Introduction

Soil serves as a major sink for heavy metals and plays a critical role in the environmental fate of these contaminants (Jayakumar *et al.*, 2021). Quarrying operations such as blasting, rock crushing, and vehicular movement release dust and particulate matter into the environment, contributing to the deposition of PTEs in nearby soils (Nieder & Benbi, 2024). In areas surrounding quarries in Akure and Ibadan, significantly elevated levels of Fe, Pb, Zn, and Cr were recorded in surface soils up to 200 meters from quarrying sites (Owolabi & Adesida, 2020). Spatial studies have shown that heavy metal concentrations generally decrease with distance from the source, but elevated levels can persist beyond 300 meters depending on wind patterns, soil porosity, and the intensity of quarry operations (Zhang *et al.*, 2020). In Gombe, soil samples collected near limestone quarrying zones exhibited moderate enrichment of metals such as Hg, Cd, and Zn, with implications for food safety and groundwater quality (Gurama *et al.*, 2020). The geochemical characteristics of soil around quarry sites not only reflect anthropogenic input but are also influenced by bedrock mineralogy, soil pH, organic matter, and texture (Singhal *et al.*, 2020). For example, a study in the Oban Massif in Southeastern Nigeria noted that older quarry zones exhibited higher contamination factors compared to newer sites due to prolonged exposure (Ekwere *et al.*, 2021). Soil analysis also reveals bioaccumulation potential in edible crops. Cassava tubers grown on quarry soils in Umunneochi were found to accumulate Pb, Zn, and Cd at levels exceeding safe dietary thresholds, indicating a clear pathway of human exposure through agriculture (Ihejirika *et al.*, 2021).

In addition, research in Ebonyi State and Riruwai, Northwest Nigeria, indicated that quarrying activities significantly altered soil properties, leading to lower cation exchange capacity, acidic pH, and reduced organic matter, which exacerbate metal mobility and toxicity (Enwere *et al.,* 2024). Ecotoxicological metrics such as Contamination Factor (CF), Pollution Load Index (PLI), and Geo-accumulation Index (Igeo) have proven effective in assessing pollution levels near quarry sites. Many Nigerian studies applying these indices have revealed contamination ranging from moderate to high, especially for Pb, Cr, and Ni, emphasizing the need for continuous soil monitoring (Oloruntoba *et al.*, 2024). Although several studies have been conducted across Nigeria, there is a lack of published research specifically evaluating soil contamination at the Rimin Gado quarry site. Given its proximity to residential areas and reliance on agricultural land, there is a critical need to assess the concentration, distribution, and risks associated with PTEs in local soils. Such an investigation would contribute essential data to guide land use, public health strategies, and environmental management in the area as the area is reported to have prevalence of cases in the recent time.

2. Materials and methods

2.1. Material

All chemical reagents used in this study were prepared using analytical-grade chemicals and deionized water. All glassware ware thoroughly cleaned with detergent, rinsed with water and acetone, and dried in an oven at 105°C (Bhuyar, 2021; El Hammari *et al.,* 2022) .

2.2. Soil collection

To obtain representative composite samples of the disturbed area, topsoil (0-20 cm) was collected in triplicate using an auger sampler as reported by (Kabala *et al.*, 2021). Furthermore, Nine (9) individual samples were collected in triplicate seven (7) from the surrounding community to capture spatial variability in soil properties. One sample was also collected as a control at about 10 kilometres away. All sampling procedures adhered to standard soil sampling protocols, ensuring systematic collection to reduce cross-contamination and maintain sample integrity. Before laboratory analysis, the collected soils were air-dried, homogenized, and sieved through a 2 mm mesh sieve.

2.3. Study Area

Rimin Gado, a local government area in Kano state, is situated approximately 20 km west of the state capital and spans an area of 225 square kilometers between the latitude of 11.965°N and the longitude of 8.25°E. The area was selected because of the recent cancer outbreak, which might be linked to the anthropogenic activities of the granite quarry that affect their drinking water. Seven sampling stations were identified in the vicinity of the quarrying sites.

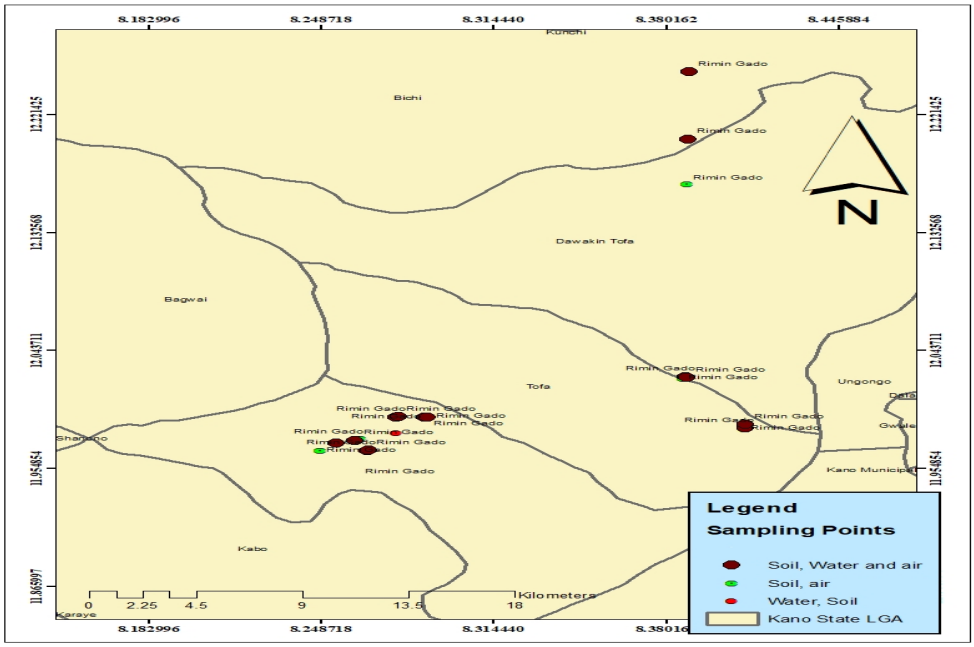

Fig 1. Map of the Area showing the sampling sites

Table 1: The Sampling Sites

SN	Name	Symbol
1	Sample point 1	ZS
2	Sampling point 2	ZD
3	Sampling Point 3	HM
4	Sampling point 4	KT
5	Sampling point 5	DG
6	Sampling point 6	BK
7	Sampling point 7	SC
8	Sampling point 8	CL
9	Sampling point 9	QS

2.4. Sequential Extraction Procedure (Conca *et al.*, 2020)

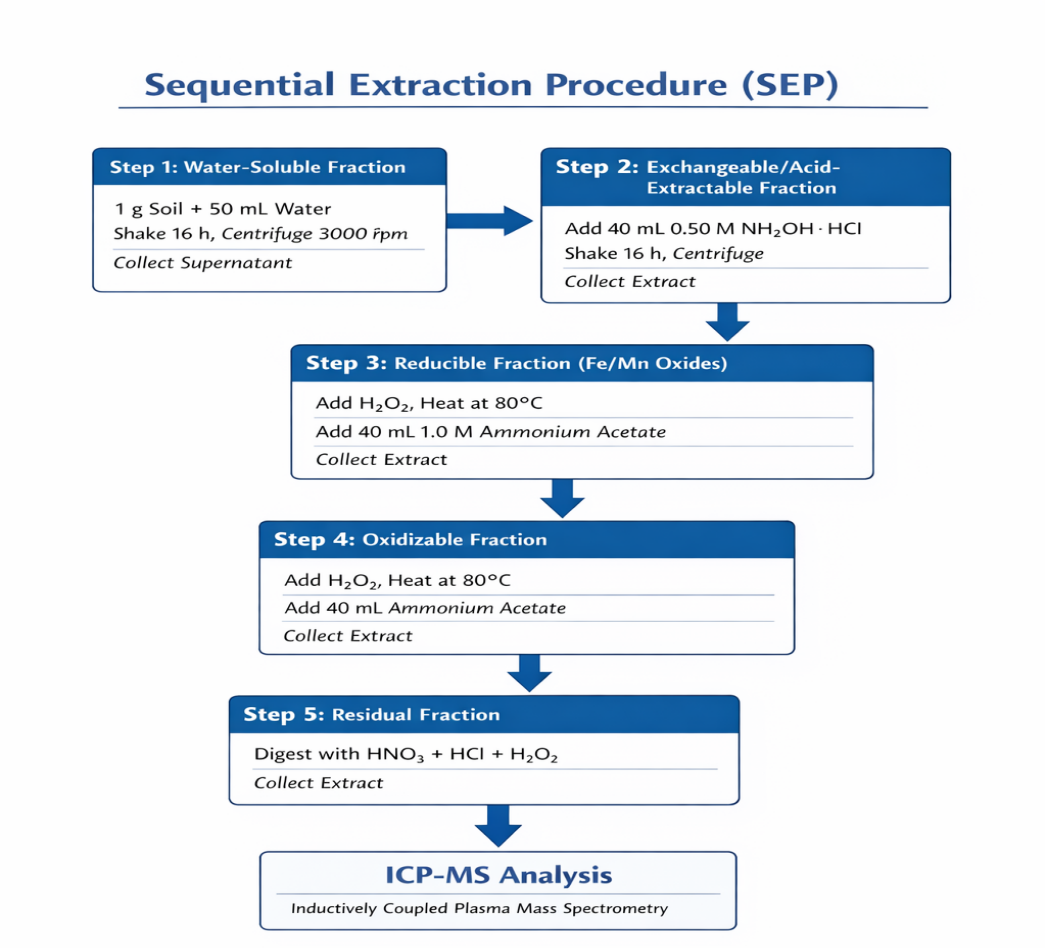

2.5. Geo-accumulation Factor (Igeo)

Müller in 1969 introduced the formula for calculating the geo-accumulation factor (Igeo) (Aung *et al.*, 2018).

$$\text{Igeo} = Log_2\left(\frac{Cn}{1.5\ Bn}\right) \quad \text{..... (1)}$$

Where

Cn is the concentration of the metal in the soil in (mg/kg)

Bn is the concentration of the metal in the background value in (mg/kg)

Igeo ≤ 0 indicates uncontaminated to low contamination

0 < Igeo ≤1 suggests moderate contamination.

1 < Igeo ≤ 2 signifies moderate to strong contamination.

2 < Igeo ≤3 represents strong contamination

Igeo > 3 indicates extremely high contamination.

2.6. Enrichment Factor

The enrichment factor was calculated using the following formula (Aytop *et al.*, 2023):

$$E_f = \frac{Cn/Cref}{Rn/Rref} \quad \text{.....(2)}$$

Where

Cn = concentration of the specific element in the sample

C_F = Background or reference element

Rn = Concentration ratio of the element to a reference element in the sample

R_{ref} = Concentration ratio of the element to a reference element in the background of reference sample.

2.7. Bioavailability

Metal bioavailability refers to the proportion of metals that can be absorbed by living organisms under normal environmental conditions. In the context of sequential extraction, bioavailability is calculated as the sum of metals in fractions that represent readily or potentially available forms in relation to the total metal concentration (Mebane *et al.*, 2020).

$$\text{Bioavailability} = \frac{FW+FEX+FRED+FOX}{FTOTAL} \times 100 \quad \text{..... (3)}$$

Where

F_w = Water Soluble Fraction

F_{ex} = Exchangeable Fraction

F_{red} = Reducible Fraction

F_{ox} = Oxidizable Fraction

F_{total} = Total Fraction

2.8. Health Risk Assessment

Health risk assessment is critical for understanding and quantifying potential health risks associated with exposure to hazardous agents or environmental conditions (Smith *et al.*, 2023).

There are three (3) ways that humans can be exposed to potentially toxic elements (PTEs).

i. Inhalation

ii. Ingestion

iii. Dermal contact

For these methods, the average daily intake, which accounts for exposure, is calculated using the following formula:

a) Average daily intake through ingestion

$$ADI_{ing} = \frac{C \times IRing \times EF \times ED}{BW \times AT} \times 10^{-6} \quad \text{..... (4)}$$

b) Average daily intake through inhalation

$$ADI_{inh} = \frac{C \times IRinh \times EF \times ED}{PET \times AT} \quad \text{..... (5)}$$

c) Average daily intake through the dermis

$$ADI_{darmal} = \frac{C \times SA \times SAF \times ABS \times EF \times ED}{BW \times AT} \times 10^{-6} \quad \text{..... (6)}$$

Where

C = Concentration of the metal

IR_{inj} = Ingestion rate

EF = Exposure frequency

ED = Exposure duration

BW = Body weight

AT = Average time

PET = Particle emission factor

SAF = Skin adherence factor

ABS = Absorption factor of skin

$ADI_{total} = ADI_{inj} + ADI_{inh} + ADI_{dermal}$

2.9. Non-Cancer Risk Assessment

It's calculated using the following equation (Smith *et al.*, 2023):

$$HQ = \frac{ADI(inh,inj,darmal)}{RfD} \quad \text{..... (7)}$$

Where HQ = Hazard quotient

R_fD = Reference dose (mg/kg/day)

Hazard Index

$$HI = HQ(inh, inj, darmal,) \text{.....(8)}$$

If HI > 10^{-6}, there is a probability of non-carcinogenic health. Imagine

2.10. Carcinogenic Risk Assessment

It's calculated using the following equation (Smith *et al.*, 2023):

$$CR = ADI \times SF \quad \text{..... (9)}$$

Where

SF = carcinogenic slope factor

$$\text{Total Carcinogenic risk} = \sum_i^1 CR = TCR \text{.....(10)}$$

$$TCR = CR_{inj} + CR_{inh} + CR_{darmal}$$

If the value of CR lies between = 1×10^{-6} to 1×10^{-4} there is no risk of cancer

2.1. Hierarchical Cluster Analysis (HCA).

Hierarchical Cluster Analysis (HCA) is a multivariate statistical method that groups samples or variables according to their similarity (El-Araby *et al.*, 2023). It computes a dissimilarity matrix (e.g., Euclidean distance) and iteratively merges similar samples using a predetermined linkage method, resulting in a dendrograms that visually depicts sample relationships (Negri, 2023).

3. Results and discussion

3.1. Results obtained from different fractions

Antioxidant activity, total phenolics and flavonoid contents

Sequential extraction procedure was used to determine concentrations of several PTE's in the soil samples as shown in Table 2 to 9

Table 2: Mean concentrations of Mn, Cu, Ni, Co, Al, and Zn in different Fractions across ZS, ZD, and HM, Standard deviation and their Rankings using Tukey HSD PostHoc

S/N	Fractions	Mn (mg/kg)	Cu (mg/kg)	Ni (mg/kg)	Co (mg/kg)	Al (mg/kg)	Zn (mg/kg)
1	ZS_W	29.20^{ab}±2.55	23.40^{b}±3.30	17.3a±2.00	25.94^{b}±1.91	55.00^{cd}±3.61	43.20^{d}±3.25
2	ZS_EX	20.6^{a}±2.20	19.12^{b}±1.68	7.18^{bc}±1.2	12.80^{a}±1.35	27.32^{a}±2.85	27.60^{c}±2.69
3	ZS_RED	27.20^{ab}±3.40	24.60^{b}±4.20	2.24^{a}±0.92	15.40^{a}±2.65	41.00^{b}±4.08	0.42^{a}±0.15
4	ZS_OX	33.90^{b}±3.98	5.70^{a}±0.60	13.20^{ac}±2.0	17.62a±1.51	46.15^{cd}±4.29	16.82^{b}±2.28
5	ZS_RES	28.30^{ab}±2.26	10.80^{a}±2.04	15.40^{c}±2.16	24.78^{b}±1.95	63.72^{d}±4.47	29.80^{c}±3.39
6	ZS_Psed	127.20^{c}±4.4	70.20^{c}±5.19	32.62^{d}±3.0	81.00^{c}±4.36	219.1^{e}±10.05	100.5^{d}±9.81
7	ZD_W	34.60^{ab}±3.91	23.00^{c}±2.52	4.00^{c}±0.60	32.74^{b}±3.55	60.74^{b}±4.36	42.92^{d}±2.62
8	ZD_EX	33.60^{a}±3.60	12.60^{b}±1.60	8.12^{b}±1.0	35.20^{b}±3.14	41.40^{a}±6.00	19.74^{bc}±3.40
9	ZD_RED	33.38^{ab}±4.45	12.20^{b}±1.21	6.38^{b}±0.61	27.40^{b}±2.33	38.90^{a}±4.00	24.84^{c}±2.98
10	ZD_OX	39.58^{c}±4.89	6.81^{a}±0.61	8.34^{a}±1.10	10.40^{a}±0.95	40.84^{a}±6.37	8.94^{a}±0.92
11	ZD_RES	28.60^{a}±1.80	3.31^{a}±1.02	33.16^{b}±2.84	31.00^{a}±4.36	58.90^{b}±4.39	13.24^{ab}±1.15
12	ZD_Psed	164.60^{a}±5.4	44.75^{d}±4.50	86.67^{d}±4.36	129.20^{c}±5.98	227.74^{c}±12.56	95.20^{e}±6.11
13	HM_W	27.40^{a}±3.20	38.34^{c}±3.78	38.00^{c}±4.0	12.00^{a}±2.35	39.50c±5.55	32.40^{c}±2.57
14	HM_EX	26.80^{a}±3.80	36.62^{c}±3.88	6.86^{a}±1.15	11.20^{a}±1.56	33.92^{bc}±2.65	24.60^{b}±2.56
15	HM_RED	32.60^{a}±2.60	25.90^{b}±1.17	16.04^{b}±2.02	15.40^{a}±0.76	14.60^{a}±1.83	5.30^{a}±0.32
16	HM_OX	31.82^{a}±3.82	28.22^{b}±2.17	35.80^{c}±2.94	19.0^{a}±2.65	24.30^{ab}±2.82	35.74^{c}±3.59
17	HM_RES	31.78^{a}±5.78	16.88a±2.04	39.04^{c}±3.08	11.60^{a}±2.09	30.92^{ab}±3.98	38.88^{c}±3.75
18	HM_Psed	137.99^{b}±5.21	125.02^{d}±5.18	123.70^{d}±5.00	56.30^{b}±7.42	132.96^{d}±8.03	122.94^{d}±5.25

The abbreviations W, Ex, Red, Ox, Res, and Psed. Stands for water soluble, exchangeable, reducible, oxidizable, residual, and pseudototal fractions of the soil samples

Table 3. Mean concentrations of Cd, Pb, Fe, As, and Cr in different Fractions across ZS, ZD, and HM, Standard deviation and their Rankings using Tukey HSD PostHoc

S/N	Fractions	Cd (mg/kg)	Pb (mg/kg)	Fe (mg/kg)	AS (mg/kg)	Cr (mg/kg)
1	ZS_W	3.00^{c}±0.55	0.0792^{b}±0.01	60.07^{c}±5.56	25.24^{c}±3.23	6.00^{b}±1.00
2	ZS_EX	1.26^{a}±0.05	0.00092^{a}±0.0001	37.14^{b}±2.01	16.53^{b}±1.96	3.73^{a}±0.24
3	ZS_RED	0.822^{a}±0.03	ND	38.22^{b}±2.3	12.86^{ab}±1.14	2.46^{a}±0.47
4	ZS_OX	0.64^{a}±0.09	ND	30.84^{b}±4.06	8.64^{a}±1.31	3.11^{a}±0.34
5	ZS_RES	2.16^{b}±0.47	0.0068^{a}±0.009	21.39^{a}±2.28	12.6^{ab}±1.64	15.03^{c}±3.00
6	ZS_Psed	5.93^{d}±0.05	0.074^{b}±0.011	171.29^{d}±3.65	64.24^{d}±3.43	29.08^{d}±1.99
7	ZD_W	0.49^{b}±0.09	0.049^{b}±0.001	41.28^{c}±3.19	36.05^{c}±2.65	10.59^{a}±0.47
8	ZD_EX	0.086^{a}±0.006	ND	26.88^{b}±2.37	20.06b±1.75	5.93^{a}±0.63
9	ZD_RED	0.05^{a}±0.012	ND	20.40^{ab}±3.98	12.09^{a}±1.59	6.11^{a}±1.05
10	ZD_OX	0.046^{a}±0.005	ND	13.38^{a}±1.73	8.05^{a}±0.87	17.8^{b}±0.86
11	ZD_RES	0.098^{a}±0.019	0.064^{c}±0.002	41.29^{c}±2.54	32.09^{c}±1.76	25.55^{b}±3.01
12	ZD_Psed	0.70^{c}±0.006	0.124^{d}±0.001	129.25^{d}±6.18	99.09^{d}±6.08	57.74^{d}±5.27
13	HM_W	1.24^{c}±0.186	0.364^{b}±0.057	41.56^{c}±3.40	22.20^{a}±1.91	12.79^{b}±1.31
14	HM_EX	0.89^{b}±0.126	0.0164^{a}±0.0017	25.98^{b}±2.01	14.08^{a}±2.01	5.21^{a}±0.81
15	HM_RED	0.46^{a}±0.025	ND	22.14^{ab}±1.62	19.58^{a}±1.80	2.61^{a}±0.36
16	HM_OX	0.41^{a}±0.036	ND	17.16^{a}±2.84	18.53^{a}±1.17	6.87^{bc}±0.7
17	HM_RES	0.49^{a}±0.10	0.08^{a}±0.0058	48.32^{c}±4.76	17.93^{a}±2.69	26.36^{c}±2.22
18	HM_Psed	3.48^{d}±0.24	0.42^{b}±0.061	149.80^{d}±3.64	81.44^{b}±6.70	41.6^{d}±5.78

The abbreviations W, Ex, Red, Ox, Res, and Psed. Stands for water soluble, exchangeable, reducible, oxidizable, residual, and pseudototal fractions of the soil samples.

ND = Not detected

Table 4. Mean concentrations of Mn, Cu, Ni, Co, Al, and Zn in different Fractions across KT, DG, and BK, Standard deviation and their Rankings using Tukey HSD PostHoc

S/N	Fractions	Mn (mg/kg)	Cu (mg/kg)	Ni (mg/kg)	Co (mg/kg)	Al (mg/kg)	Zn (mg/kg)
1	KT_W	$27.80^{a}\pm3.80$	$22.00^{bc}\pm2.80$	$41.60^{c}\pm2.44$	$36.80^{c}\pm2.23$	$42.60^{b}\pm7.06$	$43.60^{b}\pm3.81$
2	KT_EX	$35.42^{b}\pm5.22$	$14.00^{b}\pm2.00$	$23.38^{a}\pm2.40$	$11.40^{a}\pm0.78$	$39.50^{ab}\pm5.81$	$35.30^{ab}\pm2.97$
3	KT_RED	$22.40^{a}\pm4.73$	$12.74^{a}\pm2.98$	$21.80^{a}\pm2.00$	$24.22^{b}\pm4.12$	$25.70^{a}\pm2.41$	$39.54^{b}\pm4.38$
4	KT_OX	$28.60^{ab}\pm3.12$	$16.20^{ab}\pm2.20$	$33.68^{b}\pm2.24$	$17.40^{ab}\pm0.95$	$39.60^{ab}\pm6.38$	$25.00^{a}\pm2.64$
5	KT_RES	$25.36^{ab}\pm2.16$	$10.06^{a}\pm3.02$	$35.82^{bc}\pm3.91$	$20.60^{ab}\pm1.35$	$32.00^{ab}\pm5.10$	$40.60^{b}\pm3.49$
6	KT_Psed	$127.72^{c}\pm4.92$	$72.00^{c}\pm3.00$	$143.20^{d}\pm3.54$	$98.20^{d}\pm9.44$	$152.18^{c}\pm8.34$	$170.72^{d}\pm9.74$
7	DG_W	$31.38^{a}\pm1.82$	$30.40^{c}\pm4.00$	$29.00^{b}\pm4.36$	$19.80^{a}\pm4.95$	$62.60^{d}\pm2.65$	$45.68^{b}\pm2.56$
8	DG_EX	$40.56^{b}\pm4.36$	$25.10^{c}\pm1.94$	$16.68^{a}\pm2.03$	$36.74^{b}\pm2.38$	$38.90^{c}\pm4.45$	$38.80^{ab}\pm4.69$
9	DG_RED	$39.20^{b}\pm3.60$	$12.98^{ab}\pm2.48$	$13.04^{a}\pm1.96$	$31.80^{ab}\pm3.13$	$26.06^{b}\pm3.46$	$28.97^{a}\pm3.37$
10	DG_OX	$30.32^{ab}\pm4.80$	$18.02^{b}\pm1.98$	$16.86^{a}\pm2.74$	$19.86^{a}\pm3.76$	$16.68^{a}\pm1.67$	$25.64^{a}\pm3.83$
11	DG_RES	$25.00^{a}\pm2.00$	$7.54^{a}\pm0.78$	$26.20^{b}\pm2.80$	$35.30^{b}\pm3.39$	$39.68^{c}\pm6.42$	$43.56^{b}\pm3.40$
12	DG_Psed	$159.80^{c}\pm7.99$	$80.63^{d}\pm4.99$	$88.51^{c}\pm5.51$	$132.98^{d}\pm4.57$	$136.2^{e}\pm10.55$	$177.42^{c}\pm12.0$
13	BK_W	$31.18^{b}\pm2.18$	$38.84^{b}\pm4.00$	$43.24^{c}\pm2.64$	$24.66^{c}\pm2.47$	$59.60^{a}\pm4.88$	$43.34^{b}\pm7.36$
14	BK_EX	$31.00^{ab}\pm2.00$	$16.83^{a}\pm2.01$	$35.80^{b}\pm2.05$	$14.34^{b}\pm2.30$	$57.60^{a}\pm5.39$	$35.54^{b}\pm3.57$
15	BK_RED	$17.80^{a}\pm2.46$	$12.11^{a}\pm2.89$	$27.40^{a}\pm2.65$	$2.96^{a}\pm0.78$	$64.00^{a}\pm7.00$	$0.82^{a}\pm0.06$
16	BK_OX	$27.80^{ab}\pm3.80$	$11.34^{a}\pm1.58$	$28.050^{a}\pm3.27$	$22.30^{c}\pm4.00$	$50.40^{a}\pm3.42$	$5.00^{a}\pm0.65$
17	BK_RES	$28.80^{ab}\pm3.80$	$9.54^{a}\pm0.82$	$33.38^{ab}\pm1.95$	$25.44^{a}\pm3.10$	$59.60^{a}\pm8.03$	$40.60^{b}\pm3.09$
18	BK_Psed	$119.80^{c}\pm8.80$	$74.10^{c}\pm6.3$	$163.80^{d}\pm3.65$	$86.34^{d}\pm4.35$	$288.00^{b}\pm7.21$	$127.44^{c}\pm6.24$

The abbreviations W, Ex, Red, Ox, Res, and Psed. Stands for water soluble, exchangeable, reducible, oxidizable, residual, and pseudototal fractions of the soil samples.

Table 5. Mean concentrations of Mn, Cu, Ni, Co, Al, and Zn in different Fractions across KT, DG, and BK, Standard deviation and their Rankings using Tukey HSD PostHoc

S/N	Fractions	Cd (mg/kg)	Pb (mg/kg)	Fe (mg/kg)	AS (mg/kg)	Cr (mg/kg)
1	KT_W	ND	$1.324^{a}\pm0.079$	$48.48^{c}\pm3.55$	$30.92^{d}\pm1.79$	$21.80^{ab}\pm2.19$
2	KT_EX	ND	$1.00^{b}\pm0.016$	$26.18^{b}\pm2.46$	$9.32^{bc}\pm1.21$	$17.90^{b}\pm1.02$
3	KT_RED	ND	$0.28^{a}\pm0.078$	$28.08^{b}\pm1.72$	$6.294^{a}\pm0.95$	$11.34^{a}\pm1.23$
4	KT_OX	$0.0124^{a}\pm0.0029$	$0.32^{a}\pm0.037$	$12.08^{a}\pm2.00$	$4.97^{a}\pm1.67$	$20.20^{b}\pm2.15$
5	KT_RES	$0.002134^{a}\pm0.01$	$3.52^{c}\pm0.205$	$43.54^{c}\pm2.83$	$12.82^{c}\pm1.62$	$27.00^{c}\pm3.61$
6	KT_Psed	$0.134^{b}\pm0.01$	$6.40^{d}\pm0.41$	$145.68^{d}\pm3.77$	$85.04^{e}\pm2.56$	$47.60^{d}\pm3.91$
7	DG_W	$0.007^{a}\pm0.001$	$3.54^{a}\pm0.26$	$59.22^{d}\pm1.66$	$16.08^{cd}\pm1.66$	$11.04^{ab}\pm1.05$
8	DG_EX	ND	$2.60^{a}\pm0.22$	$24.24^{b}\pm1.94$	$12.08^{bc}\pm1.73$	$7.43^{a}\pm0.54$
9	DG_RED	$0.0316^{a}\pm0.001$	$2.49^{a}\pm0.17$	$43.66^{c}\pm2.57$	$8.08^{ab}\pm1.69$	$21.28^{c}\pm1.20$
10	DG_OX	ND	$1.50^{a}\pm0.16$	$14.36^{a}\pm0.95$	$4.09^{a}\pm0.56$	$14.31^{bc}\pm0.67$
11	DG_RES	$1.66^{c}\pm0.006$	$3.52^{a}\pm0.20$	$43.69^{c}\pm4.36$	$20.70^{d}\pm2.85$	$17.64^{c}\pm1.97$
12	DG_Psed	$1.20^{b}\pm0.06$	$15.96^{b}\pm2.07$	$166.32^{e}\pm6.01$	$61.13^{e}\pm8.49$	$60.75^{d}\pm3.5$
13	BK_W	$0.052^{b}\pm0.07$	$12.80^{c}\pm1.21$	56.96 ± 4.04	$8.86^{b}\pm5.22$	$18.72^{c}\pm1.92$
14	BK_EX	ND	$3.44^{b}\pm1.05$	36.34 ± 3.84	$0.56^{a}\pm1.73$	$11.14^{b}\pm0.38$
15	BK_RED	ND	$2.60^{b}\pm0.59$	32.34 ± 1.93	$1.02^{a}\pm017$	$3.76^{a}\pm0.51$
16	BK_OX	ND	$0.19^{a}\pm0.14$	24.11 ± 2.01	$0.58^{a}\pm0.03$	$3.53^{a}\pm1.01$
17	BK_RES	$0.304^{b}\pm0.03$	$3.88^{a}\pm0.006$	41.24 ± 1.62	$12.1^{c}\pm0.13$	$15.05^{ab}\pm0.75$
18	BK_Psed	$0.36^{c}\pm0.01$	$22.80^{d}\pm2.16$	179.93 ± 3.01	$22.81^{d}\pm2.56$	$41.68^{d}\pm6.75$

The abbreviations W, Ex, Red, Ox, Res, and Psed. Stands for water soluble, exchangeable, reducible, oxidizable, residual, and pseudototal fractions of the soil samples

ND = NOT DETECTED

Table 6. Mean concentrations of Mn, Cu, Ni, Co, Al, and Zn in different Fractions across SC, CT, and QS, Standard deviation and their Rankings using Tukey HSD PostHoc

S/N	Fractions	Mn (mg/kg)	Cu (mg/kg)	Ni (mg/kg)	Co (mg/kg)	Al (mg/kg)	Zn (mg/kg)
1	SC_W	29.40^{a}±3.40	35.11^{b}±2.49	30.00^{c}±4.58	12.80^{ab}±1.64	44.70^{a}±6.03	60.16^{b}±5.36
2	SC_EX	58.40^{c}±4.40	26.73^{b}±2.01	20.53^{b}±2.07	9.00^{a}±1.00	40.15^{a}±5.36	45.29^{a}±4.50
3	SC_RED	27.40^{a}±2.00	13.30^{a}±1.12	13.22^{a}±1.35	17.00^{ab}±2.00	40.56^{a}±6.94	52.60^{ab}±3.87
4	SC_OX	27.60^{a}±3.40	14.82^{a}±1.20	27.70^{c}±2.17	21.60^{c}±2.85	39.10^{a}±3.91	38.80^{a}±3.97
5	SC_RES	39.4^{b}±4.20	11.68^{a}±1.96	39.40^{d}±2.62	27.08^{d}±2.22	55.16^{a}±4.1	48.80^{ab}±4.33
6	SC_Psed	161.20^{d}±5.2	82.22^{d}±3.78	87.34^{e}±4.52	74.86^{e}±4.00	209.54^{b}±11.23	232.60^{c}±8.92
7	CT_W	33.00^{a}±2.6	24.20^{c}±2.00	29.98^{c}±2.93	11.32ab±0.71	11.40^{b}±1.42	27.80^{a}±3.04
8	CT_EX	36.80^{c}±1.80	18.84^{bc}±2.96	18.22^{b}±1.67	8.46a±0.82	6.18^{a}±0.77	30.60^{ab}±1.85
9	CT_RED	26.60^{b}±1.60	14.62^{ab}±2.22	3.59^{a}±1.21	14.29^{a}±1.13	26.603^{c}±1.45	21.80^{b}±2.08
10	CT_OX	25.00^{b}±2.00	11.40^{a}±1.51	16.24^{b}±1.83	9.80^{ab}±1.90	8.06^{a}±0.94	6.70^{a}±1.36
11	CT_RES	28.80^{b}±2.80	20.96^{bc}±1.70	19.80^{b}±1.12	13.50^{ab}±0.50	12.02^{b}±0.98	26.80^{c}±2.68
12	CT_Psed	116.60^{d}±5.51	77.58^{d}±4.18	66.32^{d}±3.79	58.20^{c}±5.06	49.44^{d}±3.51	166.58^{d}±6.19
13	QS_W	33.40^{a}±3.74	32.78^{b}±4.65	34.00^{ab}±2.68	17.13^{ab}±4.53	48.70^{a}±3.04	62.49^{b}±2.73
14	QS_EX	60.40^{c}±3.22	38.44^{b}±2.93	25.87^{b}±3.05	10.00a±2.41	42.15^{a}±3.40	46.96^{a}±3.95
15	QS_RED	30.30^{a}±4.16	33.40^{b}±3.03	14.87^{a}±1.54	18.00^{ab}±2.00	40.89^{a}±4.63	52.60^{ab}±3.87
16	QS_OX	30.93^{a}±3.30	16.48^{b}±1.53	28.70^{b}±1.60	23.10b^{c}±1.03	43.77^{a}±1.97	42.27^{a}±2.57
17	QS_RES	42.73^{b}±3.00	13.68^{a}±1.02	40.73^{c}±3.1	30.47^{c}±3.87	53.16^{a}±3.10	50.80^{ab}±5.25
18	QS_Psed	164.87^{c}±14.60	81.55^{c}±3.13	90.67^{d}±7.10	67.33^{d}±9.45	209.14^{b}±12.20	226.60^{c}±8.13

The abbreviations W, Ex, Red, Ox, Res, and Psed. Stands for water soluble, exchangeable, reducible, oxidizable, residual, and pseudototal fractions of the soil samples

Table 7: Mean concentrations of Mn, Cu, Ni, Co, Al, and Zn in different Fractions across SC, CT, and QS, Standard deviation and their Rankings using Tukey HSD PostHoc

S/N	Fractions	Cd (mg/kg)	Pb (mg/kg)	Fe (mg/kg)	AS (mg/kg)	Cr (mg/kg)
1	SC_W	0.27^{a}±0.0534	3.72^{a}±0.158	54.44^{b}±2.15	8.12^{b}±0.85	23.73^{b}±2.95
2	SC_EX	0.14^{a}±0.020	2.54^{a}±0.300	39.50^{a}±3.66	4.06^{a}±0.13	6.10^{a}±0.99
3	SC_RED	0.33^{a}±0.020	1.91^{a}±0.130	43.68^{a}±3.51	1.52^{a}±0.0.09	3.51^{a}±0.70
4	SC_OX	0.25^{a}±0.0081	2.20^{a}±0.341	38.72^{a}±2.51	4.06^{a}±0.96	7.48^{a}±0.56
5	SC_RES	2.26^{b}±0.150	16.74^{b}±0.700	34.09^{a}±2.16	12.09^{c}±1.00	39.27^{c}±4.06
6	SC_Psed	2.62^{c}±0.070	16.56^{c}±2.95	179.08^{c}±7.20	20.06^{d}±2.95	69.4^{d}±10.01
7	CT_W	ND	1.70^{b}± 0.25	8.58^{b}±0.40	4.06^{b}±0.95	7.76^{a}±0.49
8	CT_EX	ND	1.40^{b}±0.176	4.22^{a}±0.15	0.42^{a}±0.04	3.89^{a}±0.90
9	CT_RED	ND	0.35^{a}±0.027	4.63^{a}±0.58	0.52^{a}±0.08	3.05^{a}±0.05
10	CT_OX	ND	0.6^{a}±0.08	4.52^{a}±0.59	0.82^{a}±0.03	7.92^{a}±1.05
11	CT_RES	0.01296^{a}±0.010	1.20^{b}±0.35	12.30^{c}±0.68	1.22^{a}±0.10	14.36^{b}±1.09
12	CT_Psed	1.4252^{b}±0.030	3.74^{c}±0.28	33.24^{d}±2.68	8.04^{c}±1.20	19.12^{c}±4.75
13	QS_W	0.536^{a}±0.16	4.70^{a}±1.12	58.78^{b}±1.69	11.32^{b}±0.99	28.40^{b}±2.14
14	QS_EX	0.180^{a}±0.77	2.17^{a}±0.23	39.50^{a}±3.66	9.78^{a}±2.22	6.68^{a}±1.52
15	QS_RED	0.420^{a}±0.16	2.24^{a}±0.62	44.01^{a}±3.61	4.95^{a}±0.88	4.17^{a}±1.36
16	QS_OX	0.318^{a}±0.05	3.04^{a}±0.31	36.40^{a}±2.26	1.85^{a}±0.51	7.82^{a}±1.07
17	QS_RES	2.50^{b}±0.27	8.06^{b}±1.43	27.22^{a}±2.56	3.72^{b}±1.11	39.94^{c}±3.08
18	QS_Psed	3.62^{c}±0.95	17.22^{c}±3.31	192.41^{c}±10.68	22.78^{c}±3.60	64.53^{d}±5.31

The abbreviations W, Ex, Red, Ox, Res, and Psed. Stands for water soluble, exchangeable, reducible, oxidizable, residual, and pseudototal fractions of the soil samples

ND = Not Detected

The results showed that by partitioning metals into operationally defined geochemical fractions, sequential extraction sheds light on their mobility, bioavailability, and potential ecological risk. Metals were categorized as water soluble, exchangeable, reducible, oxidizable, and residual, with significant spatial variation across sampling sites (ANOVA, $p < 0.05$).

Water-Soluble Fraction (F1)

The water-soluble fraction represents the most mobile and immediately bioavailable form of heavy metals in soil, consisting of metals dissolved in soil pore water or weakly retained on particle surfaces. In the present study, the water-soluble fraction exhibited pronounced spatial variation across the sampling sites (ANOVA, $P < 0.05$), following the contamination levels as follows: QS > BK > HM > KT > SC > ZS > ZD > DG > CR. The highest concentrations were recorded at the Quarry Site (QS), with progressively lower levels observed away from the quarry, and the least concentrations at the control site (Sirbu-Radasanu *et al.,* 2025). Cadmium (Cd), Lead (Beno *et al.*), and Arsenic (As) were the dominant metals in this fraction at impacted sites, whereas Fe and Al were largely negligible in soluble form. The minimal water-soluble concentrations at CR confirm that enrichment in this fraction is predominantly anthropogenic and directly associated with quarry operations.

Geochemically, the presence of Cd and Pb in the water-soluble fraction suggests recent deposition and poor retention within the soil matrix. Metals in this fraction are extremely sensitive to variations in soil pH, electrical conductivity, and moisture content. The significant correlation between water-soluble Cd and EC indicates that increased ionic strength at quarry-proximal sites improves metal solubility. Furthermore, minor changes in soil pH influence desorption processes, allowing for greater Cd and Pb release into the soil solution. The elevated concentrations of these metals in F1 correspond to the high Enrichment Factor and Contamination Factor (CF) values for Cd and As, indicating anthropogenic input. Similar findings have been reported in quarry-impacted soils, where soluble Cd and Pb fractions were strongly associated with dust deposition and mechanical rock fragmentation processes (Serif *et al.,* 2022). The water-soluble fraction poses the greatest immediate ecological and human health risk because metals in this form are easily absorbed by plants, leached into groundwater, and consumed directly through soil contact (Nieder *et al.*, 2018). Cd, Pb, and As have higher non-carcinogenic and carcinogenic risk indices in this study, owing to their dominance in the water-soluble fraction. This fraction thus offers a direct route of exposure, particularly for children who are more prone to soil ingestion. The clear spatial gradient, significant statistical variation, and correlation with pollution indices all indicate that quarry activities have shifted metal partitioning to highly mobile forms, exacerbating environmental contamination and associated public health risks in Rimin Gado.

Exchangeable Fraction (F2)

The exchangeable fraction represents metals that are weakly adsorbed on soil particle surfaces and easily displaced by competing cations via ion-exchange processes. Although slightly less mobile than the water-soluble fraction, it is still extremely bioavailable and environmentally sensitive. In the current study, the exchangeable fraction exhibited significant spatial variation across sampling sites (ANOVA, $p < 0.05$), following the trends QS > BK > HM > KT > SC > ZS > ZD > DG > CR (Fig). Elevated concentrations were consistently recorded at QS and adjacent quarry-proximal sites, while the control site showed minimal exchangeable metal levels. Cadmium (Cd) and lead were the most common metals in this fraction, with moderate contributions from zinc (Zn), indicating significant anthropogenic enrichment. The presence of Cd and Pb in the exchangeable fraction indicates weak electrostatic binding and a high sensitivity to changes in soil chemistry, particularly pH and ionic strength. Exchangeable metals are easily mobilized in response to changing environmental conditions such as rainfall infiltration or shifts in soil acidity. The positive association observed between exchangeable metals and electrical conductivity indicate that increased ionic concentration enhances cation competition and metal displacement. Similar observations have been reported in quarry- and industrial-impacted soils where Cd and Pb were enriched in exchangeable forms due to dust deposition and mechanical disturbance (Alloway, 2013; Ogunkunle & Fatoba, 2014). The high Enrichment Factor and Contamination Factor (CF) values recorded for Cd and Pb in this study further corroborate their anthropogenic origin and labile nature. The metals in the exchangeable fraction pose substantial ecological and human health risk due to their ease of mobilization into soil solution. Their presence in this fraction contributes directly to the elevated non-carcinogenic and carcinogenic risk indices observed, particularly for Cd and Pb. The clear spatial gradient, statistical significance, and clustering of Cd and Pb within the anthropogenic group in hierarchical cluster analysis (HCA) confirm quarrying as the dominant source of exchangeable metal enrichment. Thus, the exchangeable fraction serves as a critical indicator of recent contamination and potential short-term exposure risk in the study area.

Reducible Fraction (F3)

The carbonate-bound fraction comprises metals associated with carbonate minerals and is considered a potentially mobile pool that is highly sensitive to changes in soil pH. Metals in this fraction are relatively stable under neutral to alkaline conditions, but they can be rapidly released in acidic environments. The carbonate-bound fraction varied significantly across sampling sites (ANOVA, $p < 0.05$), with mean concentrations decreasing in the following order: QS, BK, HM, KT, SC, ZS, ZD, DG, and CR. The highest concentrations were found at QS and other quarry-proximal locations, while the control site

consistently had the lowest levels. Lead, cadmium (Cd), and zinc (Zn) were the most common metals in this fraction, indicating partial stabilization via association with carbonate phases. The enrichment of Pb and Cd in the carbonate-bound fraction indicates a reaction with carbonate materials derived from granite dust and weathered quarry particulates. Although this association may temporarily reduce immediate mobility, metals in this fraction remain environmentally unstable because even slight decreases in soil pH can trigger dissolution and remobilization (Alloway, 2013). The observed relationship between soil pH and carbonate-bound metals lends support to this mechanism. Furthermore, the elevated Enrichment Factor and Geo-accumulation Index (Igeo) values for Cd and Pb are consistent with their dominance in this fraction, supporting the conclusion of strong anthropogenic input. Similar results have been reported in industrial and quarry-impacted soils, where carbonate-bound Cd and Pb served as a significant secondary reservoir of contamination (Kabata-Pendias & Pendias, 2011; Serif et al., 2022). The carbonate-bound fraction is a latent risk pool that can release metals into more mobile forms in response to environmental stressors like acidification or increased rainfall. This dynamic behaviour contributes to long-term contamination potential and accounts for some of the elevated health risk indices associated with Cd and Pb in the study area. The consistent spatial gradient, statistical significance, and clustering of Pb and Cd within anthropogenic groups in HCA all support the notion that quarry operations have increased metal accumulation in both immediately mobile and potentially mobilizable forms. Thus, the carbonate-bound fraction serves as an important transitional reservoir between stable and bioavailable metal pools in Rimin Gado's quarry-impacted soils.

Oxidizable Fractions (F4)

The Fe-Mn oxide bound fraction consists of metals associated with iron and manganese oxyhydroxides, which act as effective adsorptive surfaces in soils. This fraction is considered moderately stable under oxidising conditions, but it may become unstable in reducing environments. Metal concentrations in the Fe-Mn oxide fraction differed significantly between sampling sites (ANOVA, $p < 0.05$), with QS, HM, BK, KT, SC, ZS, ZD, DG, and CR in the order. Concentrations were highest at QS and HM, while the control site had the lowest levels. Iron and manganese dominated this fraction, but Pb, Cd, and Zn were also detected at impacted sites, indicating secondary adsorption onto oxide surfaces. The presence of Cd and Pb in this fraction suggests a preference for Fe-Mn oxides, which serve as important trace metal scavengers in soil systems. Under stable oxidizing conditions, these oxides effectively immobilize metals through adsorption and co-precipitation. Changes in redox potential, particularly under high soil moisture or waterlogging, can reduce Fe and Mn oxides, releasing previously bound metals into the soil solution (Anas *et al.*, 2026). Han *et al.* (2023) observed the relationship between moisture content and certain oxide-bound metals provide support for this mechanism. Although this fraction had high Fe

concentrations, the low enrichment factor and predominant residual presence confirm its lithogenic origin, whereas the associated Cd and Pb indicate anthropogenic inputs consistent with quarry activities similar results were reported by (Alloway, 2013). From an environmental risk standpoint, the Fe-Mn oxide fraction is a conditionally stable reservoir of metals that may contribute to secondary contamination under changing redox conditions. While less immediately mobile than the water-soluble and exchangeable fractions, its ability to release metals during environmental disturbance emphasises its long-term importance. The spatial gradient, statistical significance, and hierarchical cluster analysis (HCA), which identified Fe as primarily geogenic while grouping Cd and Pb within anthropogenic clusters, all show that quarry operations influenced not only surface adsorption processes but also deeper geochemical partitioning mechanisms. As a result, this fraction serves as a link between relatively stable and potentially mobile metal pools in the study area's soils.

Residual Fraction (F6)

The residual fraction is made up of metals that are structurally integrated into the soil matrix's primary and secondary minerals, which are typically derived from parent rock material. Metals in this fraction are considered geochemically stable and largely immobile in natural environments because they are incorporated into crystalline lattices rather than adsorbed onto particle surfaces. As a result, the residual fraction is widely regarded as the least bioavailable and environmentally reactive metal pool (Zhao *et al.*, 2020). In this study, iron (Fe) and aluminium (Al) dominated the residual fraction across all sampling sites, with other metals contributing only minor amounts. This dominance reflects the study area's granitic geology, which is naturally rich in aluminosilicate and iron-bearing minerals. Although total Fe concentrations were high, their partitioning into the residual fraction, coupled with a low enrichment factor and geo-accumulation Index (Igeo) values, confirms The origin is primarily lithogenic, rather than anthropogenic enrichment. Hierarchical cluster analysis (HCA) supported this interpretation by categorising Fe and Al separately from Cd, Pb, and As, which were associated with anthropogenic fractions. Residual metal concentrations followed a less pronounced but noticeable trend: QS ≈ BK ≈ HM > KT > SC > ZS > ZD > DG > CR. The slightly elevated residual concentrations at QS and adjacent sites are most likely due to natural rock exposure and mechanical fragmentation during quarrying, rather than contamination-induced enrichment. ANOVA revealed significant site-to-site variation ($p < 0.05$). However, the ecological impact of this variation is limited as metals in the residual fraction are not easily mobilized under current soil conditions. Environmentally, the residual fraction acts as a stable background reservoir and provides a useful baseline for distinguishing between geogenic and anthropogenic metal inputs (Wang *et al.*, 2019). The contrast between high residual Fe-Al dominance

and elevated labile fractions of Cd and Pb supports the conclusion that quarry activities changed metal partitioning rather than simply increasing total metal content. As a result, while the residual fraction itself poses little immediate ecological or human health risk, comparing it to more mobile fractions is critical for accurate source allocation and risk interpretation in the study area.

Pseudo total Metal Concentration

The pseudo-total metal concentrations obtained using aqua regia digestion give a complete estimate of the overall metal load in soils near the Rimin Gado quarry sites, representing both lithogenic and anthropogenic inputs. The results reveals pronounced spatial variability, with concentrations following a clear decreasing trend of QS > ZS > DG > HM > ZD > SC > BK > KT > CR, indicating a strong pollution gradient from the quarry source outward. The elevated levels at the quarry site (QS) are directly linked to intensive activities such as blasting, crushing, and dust generation, which enhance the release and dispersion of metal-bearing particulates into the surrounding environment (Alloway, 2013; Ogunkunle & Fatoba, 2014). In contrast, the relatively low concentrations at the control site (CR) confirm background levels and validate the significant contribution of quarrying activities to metal enrichment in the impacted zones (Li et al., 2004; Naim et al., 2023). These findings are consistent with recent studies employing sequential extraction techniques, which show that mining-impacted soils typically exhibit elevated total metal concentrations accompanied by redistribution into more reactive geochemical fractions due to anthropogenic disturbances (Salman et al., 2020; Serif et al., 2022).

The dominance of major elements such as iron (Fe) and aluminium (Al) across all sampling sites reflects the geochemical composition of the granitic parent material, indicating a predominantly lithogenic origin (Kabata-Pendias & Pendias, 2011; Alloway, 2013). These metals are naturally abundant and largely associated with stable residual fractions, suggesting limited mobility and minimal ecological risk. Conversely, trace metals including cobalt (Co), manganese (Mn), zinc (Zn), and copper (Cu) exhibit moderate concentrations and spatial variability, pointing to a combination of natural weathering and anthropogenic contributions from quarry operations and machinery emissions (Oyekunle et al., 2011; Ogunkunle & Fatoba, 2014). More importantly, toxic elements such as nickel (Ni), chromium (Cr), arsenic (As), lead and cadmium (Cd), even at relatively lower concentrations, are of significant concern due to their persistence and toxicity (Singh *et al.,* 2010; Salman *et al.,* 2020). Sequential extraction studies further reveal that metals such as Cd, Zn, and Cu are predominantly associated with exchangeable and reducible fractions**,** indicating high mobility and bioavailability, whereas Pb, Cr, and Ni tend to be associated with oxidizable and residual fractions**,** reflecting relatively lower mobility but long-term environmental persistence (Serif *et al.,* 2022; Naim *et al.,* 2023). This speciation pattern corroborates the present findings, where anthropogenic metals show greater environmental relevance despite lower

pseudo-total concentrations. The environmental implications of these findings are considerable, as elevated pseudo-total metal concentrations indicate long-term accumulation in soils, which can adversely affect soil quality, agricultural productivity, and ecosystem health (Alloway, 2013; Salman *et al.,* 2020). The consistency between these concentrations and pollution indices such as contamination factor (CF), enrichment factor (EF), and geo-accumulation index (Igeo) confirms that the study area is moderately to severely polluted (Hakanson, 1980; Serif *et al.,* 2022). Furthermore, the linkage with sequential extraction results demonstrates that a significant proportion of metals, particularly Cd, Pb, and Zn, resides in more bioavailable fractions, increasing the risk of plant uptake and transfer through the food chain (Singh *et al.,* 2010; Salman *et al.,* 2020). Soil properties such as pH, organic matter content, and cation exchange capacity also play critical roles in controlling metal partitioning and mobility, thereby influencing their environmental behavior across sampling sites (Oyekunle *et al.*, 2011; Naim *et al.,* 2023). Overall, the observed spatial distribution patterns, supported by statistical analyses, clearly identify granite quarrying as the dominant source of metal contamination, while sequential extraction evidence further confirms enhanced mobility and bioavailability of key toxic metals, underscoring the need for effective environmental monitoring and remediation strategies (Ogunkunle & Fatoba, 2014; Serif *et al.,* 2022)

Health Risk Assessment of Heavy Metals in the Soil Samples

The health risk assessment of heavy metals in the soil across the sampling sites in Rimin Gado reveals a clear spatial gradient that is heavily influenced by proximity to quarry operations. By combining non-carcinogenic and carcinogenic risk results for both environmental media, the assessment provides a more complete, recognized cumulative exposure and public health implications. Health risk assessment remains a globally recognized approach for translating environmental contamination into measurable human health outcomes, particularly in regions where untreated surface water and direct soil contact constitute common exposure pathways (Mohammed *et al.*, 2024). Non-carcinogenic risk, assessed through the Hazard Quotient (HQ) and cumulative Hazard Index demonstrated consistent disparities among sampling locations in both water and soil. The highest cumulative HI values in water were found at SC, then ZS and KT, and finally DG and BK, which had the lowest values. The spatial pattern (SC > ZS > KT > ZD > HM > BK > DG) shows how quarry runoff and direct discharge pathways affect each other. At SC and ZS, HI values surpassed the acceptable limit (HI > 1), especially among children, suggesting possible detrimental health effects with extended exposure. In soil, a similar pattern was seen, with QS having the highest HI values, followed by BK and HM, and CR and DG having the lowest risk levels. The soil risk ranking (QS > BK > HM > KT > SC > ZS > ZD > DG > CR) shows that quarry dust deposition and metal surface accumulation close by have a big effect. Cadmium (Cd) and lead were the

primary contributors to non-carcinogenic risk in both environmental media. Cd consistently had elevated HQ values due to its high toxicity coefficient and mobility in bioavailable fractions, especially in quarry-proximal soils. Pb also contributed significantly to cumulative HI, particularly among children, demonstrating its well-documented neurotoxic effects. In contrast, despite measurable concentrations, Fe, Al, and Mn contributed minimally to overall HI due to their lower toxicity weighting and dominance in residual geochemical fractions. The consistently elevated risk values noted for children relative to adults at all sampling locations further emphasize their increased physiological vulnerability and elevated exposure rates per unit body weight (Ferguson *et al.*, 2017). Carcinogenic risk assessment revealed an increased spatial differentiation among sampling sites. When it came to water, the highest carcinogenic risk values were at SC, then ZS and KT, and they got lower and lower until they reached DG and BK. CR values were higher than the acceptable lifetime risk threshold (10^{-6}–10^{-4}) at several sites, which shows that drinking contaminated surface water poses a high long-term risk of cancer. Arsenic (As) was the main cause of cancer in water, followed by Cd and chromium (Sirbu-Radasanu *et al.* , 2025). Even at sites with lower risks, carcinogenic values were still above negligible levels, which suggests that contamination was widespread. In soil, the risk of cancer followed the pattern QS > BK > HM > KT > SC > ZS > ZD > DG > CR, which again shows that proximity is very important. QS, the site closest to quarry activity, had the highest Total Carcinogenic Risk (TCR) because it had high levels of As and Cd that were available to living things. Soil carcinogenic risks were generally lower than those in water; however, sites near quarries approached or slightly exceeded acceptable limits, especially for children. This shows that soil can hold long-term carcinogenic risk because it can be accidentally ingested and then transferred to crops or groundwater systems. The assessment shows that quarry activities have greatly increased both non-carcinogenic and carcinogenic health risks in the study area. The risk level goes down as one move farther away from the quarry operations.

The Soil Geo-accumulation Index (Igeo)

By comparing the measured total metal concentrations to background values and adding a correction factor for lithogenic variability, the Geo-accumulation Index (Igeo) was used to calculate the degree of soil pollution. The overall pollution gradient followed QS > BK > HM > KT > SC > ZS > ZD > DG > CR, according to the results, which showed significant spatial variation across the sampling sites. Cd had the highest Igeo values among the eleven metals, especially at QS and BK, where the soils were moderately to heavily contaminate. Ni, Co, and Cr were typically classified as unpolluted to moderately polluted, whereas Pb and As recorded moderate pollution categories at quarry-proximal sites. Depending on the distance from quarry activity, zinc pollution ranged from mild to moderate. Fe, Al, and Mn, on

the other hand, mostly showed negative or almost zero Igeo values at all sites, indicating their dominance from natural geological sources. Strong anthropogenic enrichment is suggested by the elevated Igeo values for Cd, Pb, and As close to QS, which are probably related to mechanical rock processing and quarry dust emissions. Because they move around a lot and tend to build up on surfaces, Cd and Pb are always at the top of Igeo classifications in soils affected by mining and quarrying. The decreasing Igeo values away from QS further support atmospheric deposition as a primary dispersal mechanism.

Soil Contamination Factor (CF)

The Contamination Factor (CF) calculated provides more help in understanding how much metal was in excess compared to baseline levels. CF values exhibited statistically significant variations among sites (ANOVA, $p < 0.05$), corroborating the impact of quarry proximity on contamination intensity. Cd had the highest CF values at all the affected sites, and it often fell into the 'considerable to very high contamination' range. Pb and As were moderately contaminated at QS and BK, while Ni, Co, and Cr were generally only slightly to moderately contaminated. Zn levels were moderately high near the quarry, but they dropped to normal levels at sites that were farther away. Fe, Al, and Mn consistently exhibited CF values near unity, substantiating their primarily lithogenic provenance. The CF-based contamination ranked as follows: Cd > Pb > As > Ni > Co >Cr > Zn > Mn > Fe > Al. This ranking is in line with global studies that show that Cd and Pb are the main pollutants in quarries and mines because they come from people and are not very common in nature (Ogunkunle & Fatoba, 2014; Tchounwou *et al.,* 2012).

Soil Enrichment Factor

The enrichment factor (Alloway & control) results demonstrate pronounced spatial heterogeneity and element-specific variability in trace metal enrichment across the study area. Elevated EF values were predominantly recorded at the quarry site (QS) and the proximal location (BK, SC, HM, ZS and KT), where several elements exceeded the threshold for moderate enrichment (EF > 50). In contrast, the control site (Chatti & Majeed) consistently exhibited EF values approximating unity, indicative of baseline geochemical conditions. This spatial differentiation provides strong evidence of localized anthropogenic inputs associated with quarrying activities. Pb exhibited minor to extreme enrichment (EF <1 to > 50) especially in QS, reflecting substantial anthropogenic contributions. These elevated values are likely attributable to particulate emissions generated during blasting, crushing, and combustion of diesel engine, followed by atmospheric transport and subsequent deposition onto surrounding soils. In comparison, Ni, Co, and Cr displayed minor, moderate to extreme enrichment (EF 1 > 50), suggesting a dual control by lithogenic background and anthropogenic inputs. Zn showed only slight enrichment (EF

<25), indicating relatively limited sensitivity to quarry-derived emissions. Conversely, Fe, Al, consistently yielded EF values within the range of approximately (0.0005–1) across the study area, confirming their predominantly geogenic origin. The near-unity EF values for these elements support their conservative behavior and validate their suitability as reference elements in EF normalization. This contrast between enriched and non-enriched elements underscores the selective mobilization and accumulation of trace metals under quarry-induced environmental conditions. The relative degree of anthropogenic enrichment followed the order: Cd (>6) > Pb (2–5) > As (2–4) > Ni > Co (1–3) > Cr (1–2.5) > Zn (1–2) > Mn > Fe > Al. The markedly elevated EF values for Cd indicate very high enrichment, suggesting strong anthropogenic loading and high environmental mobility. Pb and As also show considerable enrichment, consistent with their known affinity for fine particulate matter and their tendency to accumulate in surface soils through atmospheric deposition processes. A distinct spatial attenuation pattern was observed, with EF values decreasing progressively from QS toward CR. This gradient reflects the dispersal dynamics of quarry-derived particulates and is characteristic of point-source contamination, where concentration levels diminish with increasing distance from the emission source. Such a pattern reinforces the inference that the quarry represents the dominant source of trace metal enrichment within the study area. These findings are consistent with established literature. Bhanot *et al.* (2025) documented EF values exceeding 2–5 for Cd, Pb, and As in soils impacted by mining and industrial activities, attributing these enrichments to atmospheric deposition of contaminated particulates. Similarly, Pandey *et al.* (2022) reported elevated EF values for Pb and Cd (EF > 3) in soils surrounding quarry operations in northern Nigeria, linking these to mechanical and explosive processes. Luo *et al.* (2024) also observed significant enrichment (EF > 4) of Cd, Pb, and As in mining-impacted soils, with a clear decline in EF values with increasing distance from the source. Furthermore, Bonnah *et al.* (2026) confirmed that Fe and Al typically exhibit EF values close to unity, reinforcing their classification as conservative lithogenic elements.

Bioavailability of the Metals in the Soil Samples

The proportion of metals in non-residual fractions compared to the total concentration was used to figure out bioavailability. The results showed that the bioavailable metal fractions were highest at QS and BK and got lower as they got closer to CR, which is similar to what was seen in pollution indices. Cd had the highest bioavailability percentage of all the metals. This is because it was the most common metal in water-soluble, exchangeable, and carbonate-bound fractions. Pb and As had a moderate amount of bioavailability, especially at sites close to the quarry. Ni, Co, and Cr showed moderate bioavailability that changed based on the physicochemical conditions of the soil, especially pH and redox potential. Zn had moderate mobility, but Mn's mobility was conditional on redox-sensitive Fe–Mn oxide fractions. Fe

and Al, on the other hand, were mostly linked to the residual fraction, which meant that even though the total concentrations were high, they weren't very bioavailable. This difference shows how important chemical partitioning is for understanding environmental risk. High total concentration does not inherently signify elevated ecological risk unless metals are present in bioavailable forms (Mebane *et al.*, 2020). The bioavailability ranking went like this: Cd > Pb > As > Ni > Co > Cr > Zn > Mn > Fe > Al. This pattern is in line with the health risk assessment results, which showed that Cd and Pb were the primary contributors to non-carcinogenic risk (HQ and HI) and As was the biggest contributor to carcinogenic risk (Sirbu-Radasanu *et al.* , 2025). Similar studies in quarry-affected soils have indicated significant correlations between labile metal fractions and heightened health risk indices (Raj & Alexander, 2025).

Table 6. Hierarchical cluster Analysis Results for Metals ions Across the Sampling Sites

Metal	Number of Clusters	Cluster Composition (Sampling Sites)	Source-Specific Interpretation
Manganese (Mn)	3	(ZS, ZD, HM) (KT, DG, BK) (SC, CL, QS)	Mainly controlled by natural soil processes With minimal human influence.
Copper (Cu)	2	(ZS, ZD, KT, DG) (HM, BK, SC, CL, QS)	Dominantly influenced by anthropogenic activities Such as quarrying and agriculture.
Cobalt (Co)	3	(ZS, HM, DG) (ZD, KT, BK) (SC, CL, QS)	Largely derived from natural soil minerals And parent material.
Aluminium (Al)	2	(ZS, ZD, HM, KT, DG) (BK, SC, CL, QS)	Entirely from natural lithogenic sources Within the soil matrix.
Zinc (Zn)	3	(ZS, ZD) (HM, KT, DG, BK) (SC, CL, QS)	Shows mixed origin from both natural soil components, And human activities.
Iron (Fe)	2	(ZS, ZD, HM, KT) (DG, BK, SC, CL, QS)	Naturally controlled by soil formation And iron oxide content.
Lead (Pb)	2	(ZS, ZD, HM, KT) (DG, BK, SC, CL, QS)	Primarily from anthropogenic sources Such as quarry dust and vehicle emissions.
Arsenic (As)	3	(ZS, KT, SC) (ZD, DG, CL) (HM, BK, QS)	Mainly geogenic with localized anthropogenic influence.
Chromium (Cr)	2	(ZS, ZD, HM, KT, DG) (BK, SC, CL, QS)	Predominantly derived from natural parent material.
Nickel (Ni)	2	(ZS, HM, DG, SC, QS) (ZD, KT, BK, CL)	Controlled mainly by natural mineralogical composition.

Conclusion

This study demonstrated that soils surrounding the Rimin Gado granite quarry are significantly impacted by potentially toxic elements (PTEs), with clear spatial variability controlled by proximity to quarry operations. Pseudo-total metal concentrations revealed elevated levels at the quarry site, decreasing progressively toward the control site, confirming quarrying as the primary source of contamination. Sequential extraction showed that Cd, Pb, and Zn are predominantly associated with labile fractions, indicating high mobility and bioavailability, while Fe and Al are mainly confined to the residual fraction, reflecting their lithogenic origin.

Pollution indices (CF, EF, and Igeo) consistently identified Cd as the most critical contaminant, followed by Pb and As, with evidence of moderate to very high contamination at impacted sites. Health risk assessment further revealed that non-carcinogenic risks (HI > 1) are significant, particularly for children, while carcinogenic risks for As and Cd exceed acceptable limits. The high bioavailability of these metals enhances their environmental and health significance.

References

Alloway, B. J. (2001). Soil pollution and land contamination. *Pollution: Causes, effects and control*, *Edited by Roy M. Harison* 318.

Anas, M., Khattak, W. A., Majeed, M., Hakki, E. E., & Fahad, S. (2026). Redox reactions and their influence on the nutrient availability of plants. In *Sustainable Soil Chemistry and Plant Nutrition* (pp. 195-218). Elsevier.

Aung, H. W., Htwe, K. M., & Ko, W. (2018). *Geoaccumulation and enrichment factor of some elements in soil samples* MERAL Portal].

Aytop, H., Koca, Y. K., & Şenol, S. (2023). The importance of using soil series-based geochemical background values when calculating the enrichment factor in agricultural areas. *Environmental Geochemistry and Health*, *45*(8), 6215-6230.

Beno, R. B, Over, R. R.., & Karen, R. D. (2021). Digital Transformation for Sustainability. In: Cambridge University Press, Cambridge, UK.

Bhanot, D., Jadhav, Y., Tiwari, G., & Walia, A. (2025). Environmental Implications of Heavy Metal Deposition and Particulate Matter in Coal Mining Ecosystems. *Natural and Engineering Sciences*, *10*(1), 325-339.

Bhuyar, P. (2021). Removal of nitrogen and phosphorus from agro-industrial wastewater by using microalgae collected from coastal region of peninsular Malaysia. *African Journal of Biological Sciences*.

Bhuyar, P. (2021). Removal of nitrogen and phosphorus from agro-industrial wastewater by using microalgae collected from coastal region of peninsular Malaysia. *African Journal of Biological Sciences*.

Bonnah, F. A., Novor, S., Opuni-Frimpong, E., Akoto, D. S., Acheampong, R., & Appiah, M. (2026). Heavy metal and nutrient concentrations in cocoyam leaves from mining-impacted and non-mining communities of Ahafo, Ghana: soil pollution status, bioaccumulation, and human health risks. *Environmental Monitoring and Assessment*, *198*(4), 397.

Chatti, W., & Majeed, M. T. (2022). Information communication technology (ICT), smart urbanization, and environmental quality: Evidence from a panel of developing and developed economies. *Journal of Cleaner Production*, *366*, 132925.

Conca, E., Malandrino, M., Giacomino, A., Costa, E., Ardini, F., Inaudi, P., & Abollino, O. (2020). Optimization of a sequential extraction procedure for trace elements in Arctic PM10. *Analytical and bioanalytical chemistry*, *412*(27), 7429-7440.

Ekwere, A. S., & Edet, B. B. (2021). Temporal variations of heavy metals in sediment, soil and dust particulates across the rock quarrying districts of the Oban Massif, Southeastern Nigeria. *Environmental Nanotechnology, Monitoring & Management*, *15*, 100431.

El-Araby, I. E., Moawed, S. A., Hassan, F. A., & Gouda, H. F. (2023). A combined approach of multiple correspondence analysis and hierarchical cluster analysis for profiling relationships among categorical risk predictors: A bluetongue case study. *Slovenian Veterinary Research*, *60*(25-Suppl), 307-15.

El Hammari L., Latifi S., Saoiabi S., Saoiabi A., Azzaoui K., Hammouti B., Chetouani A., Sabbahi R. (2022), Toxic heavy metals removal from river water using a porous phospho-calcic hydroxyapatite, *Mor. J. Chem.* 10(1), 62-72, https://doi.org/10.48317/IMIST.PRSM/morjchem-v10i1.31752

Enwere, C., Nwoko, C., Njoku-Tony, R., Njoku, P., Abiamere, O., & Anaga, S. (2024) Assessment of Physico-Chemical Properties of Soils Around Quarry Sites of Different Agricultural zones of Ebonyi State, Nigeria, *International Journalof Multidisciplinary Research and Publications (IJMRAP),* 7, Issue 5, 183-190

Ferguson, A., Penney, R., & Solo-Gabriele, H. (2017). A review of the field on children's exposure to environmental contaminants: A risk assessment approach. *International journal of environmental research and public health*, *14*(3), 265.

Gurama, H. M., Sani, A. A., Omotainse, S. O., & Garba, S. T. (2020). Assessment of some Essential Metals contents of limestone and soil samples from Ashaka cement factory, Funakaye Local Government Area, Gombe State, Nigeria. *Algerian Journal of Materials Chemistry*, *3*(2), 113-123.

Han, F., An, S. Y., Liu, L., Ma, L. Q., Wang, Y., & Yang, L. (2023). Simultaneous enhancement of soil properties along with water-holding and restriction of Pb–Cd mobility in a soil-plant system by the addition of a phosphorus-modified biochar to the soil. *Journal of Environmental Management*, *345*, 118827.

Ihejirika, C. E., Ndubuisi, E. C., Njoku, J. D., Emereibeole, E. I., Ebe, T. E., Njoku-Tony, R. F., ... & Ursula, N. N. (2021). Heavy metal contamination of cassava (Manihot esculentum) grown on quarry soils in Umunneochi Abia state and its health implications. *EQA-International Journal of Environmental Quality*, *45*, 1-9.

Jayakumar, M., Surendran, U., Raja, P., Kumar, A., & Senapathi, V. (2021). A review of heavy metals accumulation pathways, sources and management in soils. *Arabian Journal of Geosciences*, *14*(20), 2156.

Kabala, C., Galka, B., & Yurkouski, S. (2021). New topsoil sampler for the assessment and monitoring of forest soil contamination. *Forests*, *12*(1), 79.

Luo, F., Zhang, F., Zhang, W., Huang, Q., & Tang, X. (2024). Distribution, ecological risk, and source identification of heavy metal (loid) s in sediments of a headwater of Beijiang River affected by mining in southern China. *Toxics*, *12*(2), 117.

Mebane, C. A., Chowdhury, M. J., De Schamphelaere, K. A., Lofts, S., Paquin, P. R., Santore, R. C., & Wood, C. M. (2020). Metal bioavailability models: Current status, lessons learned, considerations for regulatory use, and the path forward. *Environmental Toxicology and Chemistry*, *39*(1), 60-84.

Mohammed, A. B., Bioltif, Y. E., Dahiru, S. W., Babanyaya, A. M., Mustapha, A. B., Adam, A. B., & Abubakar, M. Y. (2024). Exposure pathways and risk assessment of soil pollution and human

health: a review. *Tropical journal of engineering, science and technology*, *3*(2), 35-55.
Negri, R. G. (2023). Dendrogram. In *Encyclopedia of Mathematical Geosciences* (pp. 271-274). Cham: Springer International Publishing.
Nieder, R., Benbi, D. K., & Reichl, F. X. (2018). Role of potentially toxic elements in soils. In *Soil components and human health* (pp. 375-450). Dordrecht: Springer Netherlands.
Nieder, R., & Benbi, D. K. (2024). Potentially toxic elements in the environment–a review of sources, sinks, pathways and mitigation measures. *Reviews on Environmental Health*, *39*(3), 561-575.
Oloruntoba, A., Omoniyi, A. O., Shittu, Z. A., Ajala, R. O., & Kolawole, S. A. (2024). Heavy metal contamination in soils, water, and food in Nigeria from 2000–2019: A systematic review on methods, pollution level and policy implications. *Water, Air, & Soil Pollution*, *235*(9), 586.
Owolabi, A., & Adesida, P. (2020). The Environmental and Health Implications of Quarrying Activities in the Host Community of Oba-Ile in Akure, Nigeria. *Journal of Human Environment and Health Promotion*, *6*(1), 6-10.
Pandey, V. C., Ahirwal, J., Roychowdhury, R., & Chaturvedi, R. (2022). *Eco-restoration of mine land*. John Wiley & Sons.
Raj, A. S., & Alexander, T. J. E. S. (2025). Tracing the Environmental Footprint of Abandoned Quarries: Hydro-Geochemical and Soil Quality Assessment in Kollam, India. *Tropical journal of engineering, science and technology*, *4*(2), 754.
Singhal, A., Goel, S., & Sengupta, D. (2020). Physicochemical and elemental analyses of sandstone quarrying wastes to assess their impact on soil properties. *Journal of environmental management*, *271*, 111011.
Sirbu-Radasanu, D. S., Huzum, R., Dumitraş, D. G., Stan, C. O., & Marincea, Ş. (2025). Soil geochemistry and manganese contamination risk in the abandoned mining area–Eastern Carpathians. *Environmental Geochemistry and Health*, *47*(12), 550.
Smith, K., Fearnley, C. J., Dixon, D., Bird, D. K., & Kelman, I. (2023). *Environmental hazards: assessing risk and reducing disaster*. Routledge.
Wang, S., Wang, W., Chen, J., Zhao, L., Zhang, B., & Jiang, X. (2019). Geochemical baseline establishment and pollution source determination of heavy metals in lake sediments: A case study in Lihu Lake, China. *Science of the Total Environment*, *657*, 978-986.
Zhang, Q., & Wang, C. (2020). Natural and human factors affect the distribution of soil heavy metal pollution: a review. *Water, air, & soil pollution*, *231*(7), 350.
Zhao, L., Yan, Y., Yu, R., Hu, G., Cheng, Y., & Huang, H. (2020). Source apportionment and health risks of the bioavailable and residual fractions of heavy metals in the park soils in a coastal city of China using a receptor model combined with Pb isotopes. *Catena*, *194*, 104736..